

Turbulence evolution in MHD plasmas

M. Wisniewski ^{*}, R. Kissmann [†] and F. Spanier ^{‡§}

February 19, 2022

Turbulence in the interstellar medium has been an active field of research in the last decade. Numerical simulations are the tool of choice in most cases. But while there are a number of simulations on the market some questions have not been answered finally. In this paper we are going to examine the influence of compressible and incompressible driving on the evolution of turbulent spectra in a number of possible interstellar medium scenarios. We conclude that the driving not only has an influence on the ratio of compressible to incompressible component but also on the anisotropy of turbulence.

1. Introduction

Turbulence in the context of the interstellar medium (ISM) was for the first time discussed by von Weizsäcker (1951). This discussion, however, was soon abandoned by the scientific community. Until the late seventies there was not much progress in the field of interstellar turbulence. Only when the observational techniques became better at this time it became clear that there were power law correlations between different structures in the ISM. At first turbulence was only connected to the smallest scales of the ISM but with improved observations it was found that turbulence was present at all spatial scales. A corresponding spectrum of the density fluctuations can, e.g., be found in Armstrong *et al.* (1995).

Besides the well known density fluctuation spectra also velocity power spectra may be obtained. One possible method for this has been presented by Lazarian & Pogosyan (1997) and was applied by Padoan *et al.* (2006). The connection between the velocity and density observations are not fully understood, as pointed out by Klessen (2000). For the case of the magnetic field structure functions may be observed with radio telescopes (e.g., Haverkorn *et al.*, 2004). For a more detailed account of the observational evidence for interstellar turbulence see Elmegreen & Scalo (2004).

^{*}Lehrstuhl für Astronomie, Universität Würzburg, Emil-Fischer Str. 31, D-97074 Würzburg

[†]Institut für Astro- und Teilchenphysik, Universität Innsbruck

[‡]Lehrstuhl für Astronomie, Universität Würzburg, Emil-Fischer Str. 31, D-97074 Würzburg

[§]Email address for correspondence: fspanier@astro.uni-wuerzburg.de

Since there are yet no in-situ measurements of the interstellar medium, a number of questions is still not resolved. One of those is the question of compressibility. Many theories assume an incompressible medium, yet this is not compatible with the density fluctuation observations in the ISM. In the wave picture of interstellar turbulence (Lazar *et al.*, 2003; Spanier & Schlickeiser, 2005) it may well be assumed that up to certain wave numbers a major compressible component is present. Another issue which is not yet fully answered is the question of the driving of the turbulence. The energy balance of the interstellar medium suggests that supernovae are the driving force and energy is dissipated at small scales. Whether this driving is compressible or incompressible is not clear. On the one hand the driving scenario involving supernova shock waves is connected to compression, since the shocks themselves are compressed. On the other hand streaming cosmic rays may be also a source of driving especially through incompressible Alfvén waves (Skilling, 1975).

In the course of this paper we will come back to the main theories for anisotropic MHD turbulence and review recent simulations. We then present the results of our simulations and their implications for the understanding of compressible MHD turbulence.

In this paper we will at first discuss the current knowledge about the theory of plasma turbulence, then we will present our numerical methods. The results are shown for short time scales of turbulent driving, the evolving spectrum during driving and the saturated spectrum.

2. Theory

2.1. Turbulence theory

From the theoretical side the discussion about a turbulence theory started out from the investigation of incompressible turbulence described by the Navier-Stokes equation. The early discussions by Kolmogorov (see, e.g., Kolmogorov, 1941) used the assumption of spatially homogeneous turbulence. Later on, however, it was found that intermittency had to be taken into account leading to a slightly different form of the velocity spectrum. For different intermittency models and a general overview of the turbulence see Frisch (1995). For the turbulence in a magnetised fluid the model by She & Leveque (1994) was extended to include compressibility and a magnetic field. Politano & Pouquet (1995) have discussed the role intermittency in the solar wind, proposing sheet like structures (also discussed in Grauer *et al.*, 1994).

The next important step is the inclusion of a background magnetic field. In Shebalin *et al.* (1983) numerical studies have been conducted showing anisotropies of MHD plasmas due to the background field. This aspect was addressed by Sridhar & Goldreich (1994), where the authors use a heuristic wave-model to get some idea of the anisotropy of the turbulence spectrum of magnetic turbulence with a background field. The effects of a background magnetic field, however, are by no means fully understood. This is reflected by the debate started in Goldreich & Sridhar (1995), where a discussion about the correct description of parallel and perpendicular cascades started. Another aspect is the question when turbulence can be described by a wave-interaction picture and when

non-linear processes dominated instead.

To resolve this question a number of simulations have been conducted in the last 15 years. The first numerical test has been conducted by Cho & Vishniac (2000), a prominent example are the simulations by Maron & Goldreich (2001), who consider simulations of decaying incompressible turbulence. The incompressible plasma attracts far more attention by modellers for a number of reasons: A prominent one is that incompressible plasmas may be simulated with spectral methods providing a spectrum extending to high wave numbers. Apart from that basic turbulence theories are mainly developed for incompressible fluids. But also Chandran (2005) has done additional work on compressible turbulence in the $\beta \ll 1$ limit for the evolved spectra. Due to the very low β limit sound waves are neglected in these simulations. Here, however, we will show the importance of sound waves in the context of compressible plasmas. A work which is more closely related to ours is the one of Kuznetsov (2001), where the authors investigate compressible plasmas with high and low values of β . In his approach only weak turbulence is considered. As mentioned above it is not yet clear if a wave-picture is applicable, but in the weak turbulence limit the wave-picture is explicitly assumed. Additionally a theoretical description including major cooling and damping mechanisms for the interstellar medium has been presented by Lithwick & Goldreich (2001). Here different β regimes are discussed.

2.2. Excitation of MHD waves with compressible or incompressible distortions

In Federrath *et al.* (2008, 2010) a discussion similar to our discussion regarding the influence of compressible versus incompressible driving has been started. But this discussion was limited to hydrodynamic simulations of the interstellar medium. A more recent paper (Federrath *et al.*, 2011) added the magnetic field and discussed the effect of turbulent magnetic field growth. We will extend this discussion in the case of magnetised fluids to the anisotropies present in the driven turbulence. This discussion has been continued by Lemaster & Stone (2009), who did simulations of MHD plasmas, but limited themselves to incompressible driving but with variations of the peak wave number of the driver. In their work it was shown that approximately a factor of 128 between the driving peak and the total resolution is sufficient for convergence.

2.2.1. Compressible driving

We inject compressible disturbances isotropically into our simulation domain. These disturbances can distort the magnetic field and so excite waves. The induction equation shows us which waves can be expected. Without loss of generality the preferred direction of the magnetic field can be chosen to be the x -direction (defined by the unit vector \vec{e}_x). For the induction equation we find that:

$$\frac{\partial \vec{B}}{\partial t} = -\nabla \times \vec{E} = \nabla \times (\delta \vec{v} \times B \vec{e}_x) \quad (1)$$

Where we used $\vec{E} = -\delta\vec{v} \times \vec{B}$ for the electric field which holds for ideal plasmas. If the compressible fluctuations are in x -direction no magnetic field will be injected as $(\delta v \vec{e}_x \times \vec{B} \cdot \vec{e}_x) = 0$. If the distortion is perpendicular to the background field (e.g. $\delta\vec{v} = v\vec{e}_y$) this results in a distortion of the magnetic field in x -direction:

$$\frac{\partial \vec{B}}{\partial t} = ik\vec{e}_y \times (\delta v \vec{e}_y \times B\vec{e}_x) \quad (2)$$

$$\begin{aligned} \frac{\partial \vec{B}}{\partial t} &= ik\vec{e}_y \times (-v)B\vec{e}_z \\ \frac{\partial \vec{B}}{\partial t} &= -i\vec{e}_x kvB \end{aligned} \quad (3)$$

Where we used $\nabla = ik\vec{e}_y$ as for compressible waves \vec{k} is parallel to $\delta\vec{v}$

For the case $\delta\vec{v} = v\vec{e}_z$ we also find a distortion of the magnetic field in x -direction:

$$\frac{\partial \vec{B}}{\partial t} = i\vec{e}_x kvB \quad (4)$$

As the distortion of the magnetic field is perpendicular to \vec{k} , we would expect to find compressible waves that propagate in perpendicular direction with respect to the mean magnetic field. We can also identify these waves as for MHD-waves the propagation in the perpendicular direction is only possible for fast magnetosonic waves.

2.2.2. Incompressible driving

Here we want to figure out if Alfvén waves being the only incompressible waves in MHD-plasmas can be generated from those incompressible fluctuations. As for incompressible fluctuations \vec{k} is parallel to the background field $\nabla = k\vec{e}_x$. So we find for the magnetic field:

$$\frac{\partial \vec{B}}{\partial t} = k\vec{e}_x \times (\delta v \vec{e}_y \times B\vec{e}_x) = \vec{e}_y kvB \quad (5)$$

or

$$\frac{\partial \vec{B}}{\partial t} = k\vec{e}_x \times (\delta v \vec{e}_z \times B\vec{e}_x) = \vec{e}_z kvB \quad (6)$$

As the distortion of the magnetic field is perpendicular to \vec{k} this results in Alfvén waves propagating parallel with respect to the mean magnetic field.

2.3. Three wave interaction

Three wave interaction is used to describe the interaction of compressible and incompressible waves in a weakly turbulent plasma and has been described in the first place by Chin & Wentzel (1972). Applications to high- and low-beta plasmas are discussed in Vainio & Spanier (2005).

For our investigations where we either drive with pure compressible or pure incompressible fluctuations one has to put the question with which process compressible fluctuations

are generated from incompressible fluctuations and the other way around. As this happens for small turbulent amplitudes we claim that three wave interactions are the key process.

Here a validation is carried out how Alfvén waves are generated by fast magnetosonic waves. It is also shown what can be predicted about the propagation direction of the resulting Alfvén waves. The calculation of the generation of fast magnetosonic waves from Alfvén waves can be done analog.

In principle Alfvén waves can be generated from fast magnetosonic waves by one of these two processes:

$$A^+ + F^- \leftarrow A^\pm \quad (7)$$

$$A^+ + A^- \rightarrow F^\pm \quad (8)$$

Here we will restrict the discussion to the special case of perpendicular propagating fast magnetosonic waves with $\beta \ll 1$. For this we find the phase velocity of these waves to be:

$$v_{ph} \approx (\sqrt{1 + \beta})v_A \quad (9)$$

In this case the reaction equation Eq. 9 provides no valid solution when computing the resonance condition (i.e., the energy equation). For reaction equation 8, however, we find the following resonance condition:

$$v_A(k_{A,\parallel}^+ + k_{A,\parallel}^-) = v_A(\sqrt{1 + \beta})k_F^\pm \quad (10)$$

$$v_A(k_{A,\parallel}^+ + k_{A,\parallel}^-) = v_A(\sqrt{1 + \beta})((k_{A,\parallel}^+ - k_{A,\parallel}^-)^2 + k_{F,\perp}^\pm)^{1/2} \quad (11)$$

with

$$k_{A,\parallel}^+ - k_{A,\parallel}^- = \pm k_{F,\parallel}^\mp k_{A,\perp}^+ + k_{A,\perp}^- = \pm k_{F,\perp}^\mp \quad (12)$$

As the fast magnetosonic waves propagate in the perpendicular direction $k_{F,\parallel} = 0$ and so with equation 11 and 12 we find for the parallel component of the fast magnetosonic waves:

$$k_{A,\parallel}^+ = k_{A,\parallel}^- = \frac{1}{2}k_{F,\parallel}\sqrt{1 + \beta} \quad (13)$$

For the perpendicular component of the fast magnetosonic waves we find

$$\langle k_{A,\perp}^\pm \rangle = \frac{1}{2}k_F \quad (14)$$

With that we find that

$$\tan \theta = \frac{k_{A,\parallel}}{k_{A,\perp}} = \frac{\frac{1}{2}k_F\sqrt{1 + \beta}}{\frac{1}{2}k_F} = \sqrt{1 + \beta} \quad (15)$$

where θ is the angle between the propagation direction of the fast magnetosonic waves and the Alfvén waves. As $\beta \ll 1$ it can be followed that $\tan \theta \approx 1$. This gives us a preferred propagation direction for the Alfvén waves close to $\theta = 45$ degree.

A similar study has been undertaken by Chandran (2008) for the low- β case taking into account also fast magnetosonic wave. Lithwick & Goldreich (2001) have discussed systems with high and low β , their approach is an analytical one.

3. Numerical Simulations

3.1. MHD equations

For our studies we used the ideal MHD equations in a periodic domain, where the system is closed by an isothermal equation of state. Since our analysis is a principle one we will give all variables in non-dimensional, normalised units. For that purpose all variables are split into a dimensionless variable of order unity and a normalisation constant. Here we use four independent variables for the normalisation: The length of the simulation domain L , the mass of the hydrogen atom m_0 , a typical number density n_0 , and the temperature of the system T_0 which directly relates to the speed of sound c_s . Therefore length scales are normalised as $x = L\tilde{x}$, velocity as $u = u_0\tilde{u} = c_s\tilde{u}$, density as $\rho = m_0n_0\tilde{\rho}$ and so forth. The resulting set of normalised MHD-equations is the following:

$$\frac{\partial \rho}{\partial t} = -\nabla \vec{s} \quad (16)$$

$$\frac{\partial \vec{s}}{\partial t} = -\nabla \left(\frac{\vec{s}\vec{s}}{\rho} + \left(p + \frac{B^2}{2} \right) \mathbf{1} - \vec{B}\vec{B} \right) + \vec{F} \quad (17)$$

$$\frac{\partial \vec{B}}{\partial t} = -\nabla \left(\frac{\vec{s}\vec{B} - \vec{B}\vec{s}}{\rho} \right) \quad (18)$$

$$p = \frac{c_s^2}{u_0^2} \rho \stackrel{(here)}{=} \rho \quad (19)$$

Here ρ is the mass density, $\vec{s} = \rho\vec{v}$ is the momentum density and \vec{B} indicates the magnetic induction and p is the thermal pressure. The isothermal equation of state – Eq. (19) – is simplified due to our choice for the normalisation constants.

In the following we will classify our results on the basis of β we used for our simulations. We only use it for the initialisation of the unperturbed background magnetic fields. It is defined as the fraction of the thermal and magnetic pressure.

3.2. Numerical model

For the time evolution of the MHD-equations we use a second order CWENO (Centrally Weighted Essentially Non-Oscillatory) algorithm (see e.g. (Kurganov & Levy, 2000)). It is very convenient for the simulation of shocks as we find them in fluids and plasmas. In the mathematical description these shocks are so called “Riemann Problems” and their accurate numerical treatment with a Godunov solver results in high numerical costs. The CWENO scheme avoids to solve these Riemann Problems directly by averaging over the appropriate fractions of every cell. Additionally oscillations are suppressed by the reconstruction. This results in a fast scheme for the treatment of the MHD equations with passable small dissipation. This CWENO method is combined with a third order Runge-Kutta algorithm which has been chosen because of the small memory costs with comparatively high resolution in time, due to the fact that only one additional field has to be buffered.

Besides the direct numerical simulation (DNS) technique also the large eddy simulation. This is for example demonstrated in Chernyshov *et al.* (2007, 2009) for the case of decaying turbulence. We are refraining from using this method since it requires a number of implications on the turbulent cascade on small scales which we are not sure of.

3.3. Turbulence driver

For the external stirring of the fluctuations we define a function f in Fourier space with

$$f_k = s \cdot k^{-7/4} \exp(2\pi i p) \quad (20)$$

where “ s ” and “ p ” are random numbers between zero and one. The random number generator for the former of these obeys a Gaussian distribution, whereas the latter is uniformly distributed. This function f_k yields the Fourier space distribution of the velocity fields used for driving the fluctuations in our simulations. After transforming to configuration space $f_k \rightarrow f_x$ we make the distinction between the cases of compressible and incompressible driving. For the former we use $\vec{\delta v} = \nabla f_x$, whereas for the latter we employ $\vec{\delta v} = \nabla \times \vec{f}$. As \vec{f} has, thus, to be a vectorial function in the case of incompressible driving we define each component separately with different random numbers. Each component of the wave-vector \vec{k} in our Fourier space spectra ranges from one to eight yielding a maximum absolute value of $|\vec{k}| \leq 13$. The perturbations are set up in a form such that no net momentum is added to the numerical domain. The energy input is normalised to an estimate for the average energy input by supernovae into the ISM of our Galaxy into a volume of the size of the simulation domain. The resulting driving spectrum is isotropic and it yields $v^2(k) \propto k^{-3/2}$ which yields a production spectrum harder than the anticipated inertial spectrum.

Finally we define the compressible and incompressible energy spectra. Both are calculated in Fourier space on the basis of the velocity fields with

$$P_{comp}(k) \equiv \frac{1}{2} \left\| \hat{k} \cdot \vec{v}(\vec{k}) \right\|^2 \quad (21)$$

$$P_{incomp}(k) \equiv \frac{1}{2} \left\| \hat{k} \times \vec{v}(\vec{k}) \right\|^2. \quad (22)$$

where \hat{k} is the normalised wave vector. The overall energy spectrum of the velocity fields is

$$P_K(k) \equiv \frac{1}{2} v^2(k) \quad (23)$$

where the sum of $P_{comp}(k)$ and $P_{incomp}(k)$ is $P_K(k)$. For the following discussion we have to make an important differentiation: P_K is the power spectrum of velocity fields in the whole system, whereas P_K^* is the power spectrum of the velocity fields of the driver. This is important because the turbulent energy of the velocity fields of the whole system

doesn't have to accord to the driving spectrum. This will be important in chapter 4.1.2. Additionally we define the omnidirectional energy spectrum of the magnetic fields with

$$P_B \equiv \frac{1}{2\rho} \delta B^2(k). \quad (24)$$

3.4. Simulation setup

For all our investigations we use in principle the same simulation setup: We start out from an unperturbed plasma with a homogeneous background magnetic field and inject with each time step either compressible or incompressible energy with our turbulence driver explained in section 3.3. We do this for compressible and also for incompressible driving and both runs are performed for $\beta=0.01$ and $\beta=10$. This enables us to analyse the influence of the different drivings on as well the highly magnetised as the quite hydrodynamic plasmas. So the basis of the following research are those four runs. With the simulation output we gain during the simulation we calculate the turbulent energy spectra defined in section 3.3.

4. Results

Here we will discuss three distinct topics relating to our simulation results: First we investigate the physics on short and intermediate timescales where the fluctuations of the velocity fields excite modes. This is done in section 4.1. Then the time evolution of the energies is studied in section 4.2. Finally an investigation of the convergence range is done in section 4.3. In order to quantify the anisotropy we use a scalar parameter which is derived from 2D spectra. The parameter is described in detail in A.

4.1. Short time scales

This investigation is of special interest because it can be observed how the first waves are generated for compressible as well as for incompressible driving and how these waves interact with each other. On the basis of this research we can determine which processes dominate the turbulence for small amplitudes of the fluctuations. When taking the supernova injection scenario for granted, the build-up of turbulence is a transient phenomenon which may even be observed close in time and space to the energy source. One observable could be accelerated particles in the upstream of supernova and their respective electromagnetic emission.

For the investigation of the two dimensional spectra we need to keep in mind that after this short amount of time we have to distinguish between the driving region that is dominated by the driving spectrum injected for each time step and the part of the spectrum that can only be reached via a cascade. After this short amount of time the cascading process has only taken place to some extent so we concentrate mostly on the driving region. Via the intersection points of the contour lines with the k_{\perp} - and k_{\parallel} -axes we can access the anisotropy of the turbulent fields.

4.1.1. P_B

Figures 1(a) to 1(d) show the two dimensional spectra of P_B . We see for both drivings and values of the plasma- β a very anisotropic spectrum ($k_{\perp}^{\text{aniso}}(1) = 2$) within the driving range. The spectra show a remarkable feature: For incompressible driving contour lines in the driving range rise from the k_{\perp} axis (following the diagonal), while for compressible driving the contour lines rise from the k_{\parallel} axis. The slope of the contour lines indicates a spectrum which has in parts a positive exponent with respect to k .

There is an explanation for this behaviour, which may be deduced from the fact, that the difference exist between compressible and incompressible fluctuations. For the case of incompressible fluctuations, the vector $\vec{\delta v}$ is perpendicular to the wave vector \vec{k} , while for compressible fluctuations, the both vectors are aligned. If we examine now the induction equation for incompressible fluctuations (Eq. 5) moving in parallel direction, we find

$$\frac{\partial \vec{B}}{\partial t} = \nabla \times (\delta v \vec{e}_y \times B_0 \vec{e}_x) \quad (25)$$

this yields for the turbulent velocity spectrum

$$\frac{\partial \vec{B}}{\partial t} = k_{\parallel} k^{-3/4} B_0 \quad (26)$$

This yields a rising spectrum in parallel spectrum as seen above. It also explains the crossing of the contour line and the k_{\perp} axis. For the compressible driving the explanation follows the same line, but is essentially different, since the vector $\vec{\delta v}$ has a different orientation.

We can make further distinction between $\beta = 0.01$ and $\beta = 10$: If we examine the 2D spectra closely we find a cutoff in some of the spectra, which may be identified by very close contour lines (as for example in Fig. 1(a)). For compressible driving we find a strong cutoff for $\beta = 10$, while it seems to have dissolved already for $\beta = 0.01$. Since the induction equation makes no distinction between the two values of β it seems that another physical process is taking place here. By examining P_{Comp} and P_{Shear} we will show later that this may be caused by a mixture of Alfvén and fast magnetosonic waves.

In 2(a) to 2(d) the magnetic field after a normalised time of $5 \cdot 10^{-3}$ can be seen. One may now compare the eddy size and spectrum (as done for example in Beresnyak & Lazarian 2009) to see at least qualitatively that the elongation of the eddies is correlated with the cutoff seen in the two-dimensional spectra. This is of course not unexpected.

4.1.2. P_K

Figure 3(a) to 3(d) show the two dimensional spectra of P_K for $\beta=0.01$ and $\beta=10$ for both compressible and incompressible driving.

For $\beta=0.01$ and incompressible driving we see in the driving region of P_K a perpendicular preferred direction ($k_{\perp}^{\text{aniso}}(1.5) = 1.8$) whereas for $\beta=0.01$ and compressible driving we find a parallel preferred direction ($k_{\perp}^{\text{aniso}}(1.5) = 1.5$) although P_K^* is for both cases isotropic. The term “preferred direction” is used here when the two dimensional spectra

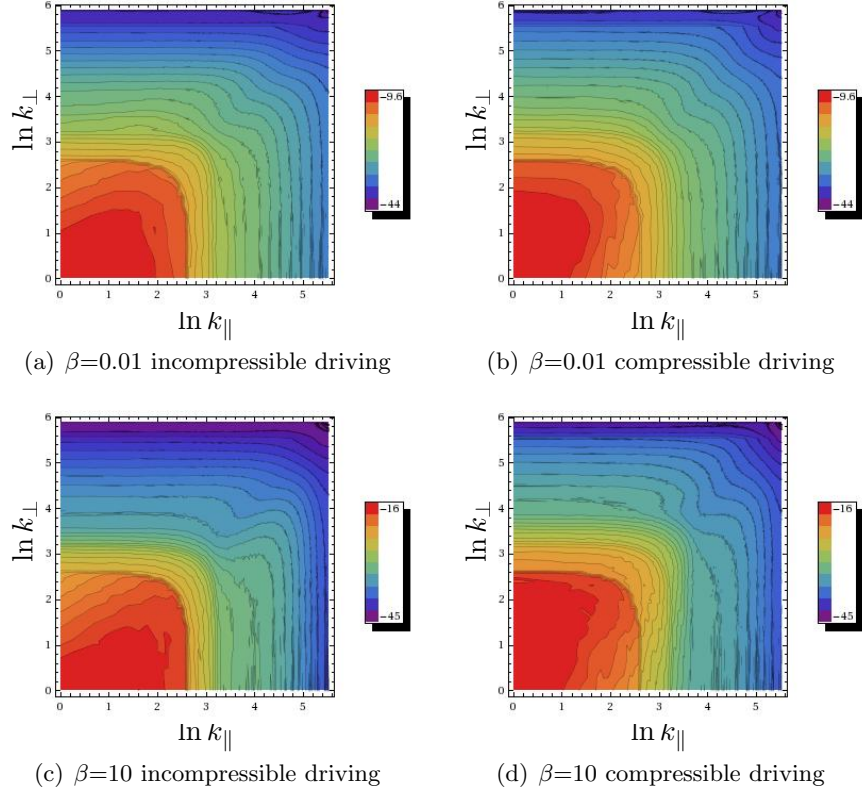


Figure 1: Turbulence spectra P_B after $t = 5 \cdot 10^{-3}$ simulated on a 512^3 grid. The color denote the natural logarithm of the numerical energy.

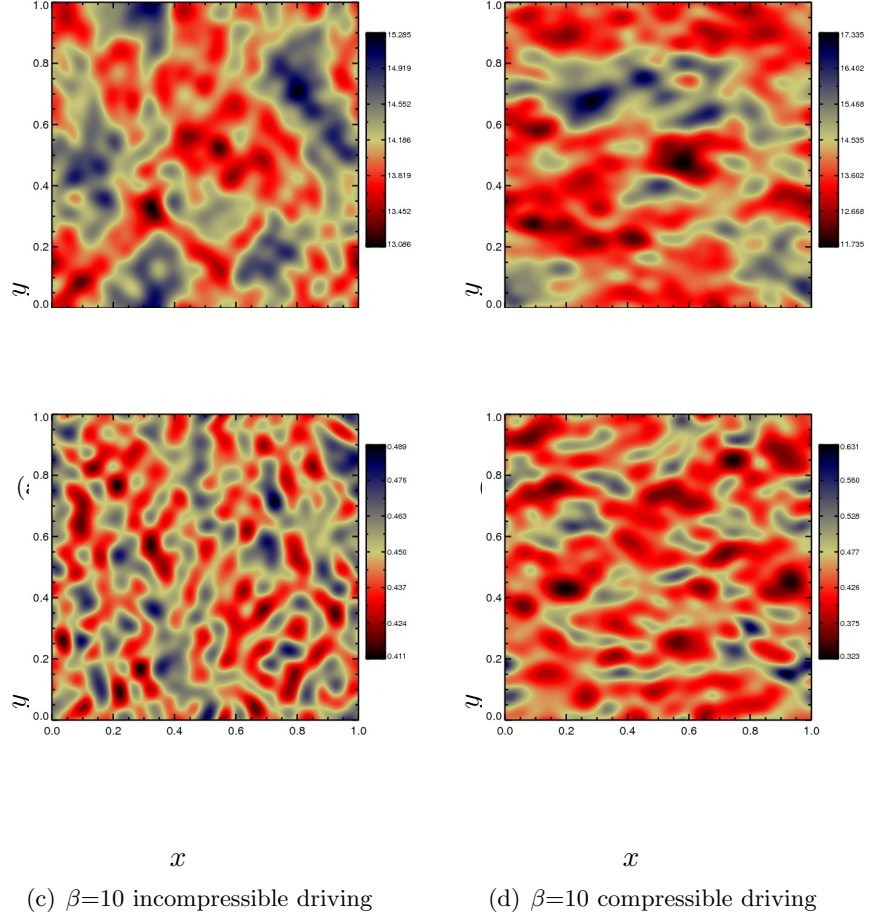


Figure 2: Turbulent magnetic fields after $t = 5 \cdot 10^{-3}$ in real space on a 512^3 grid.

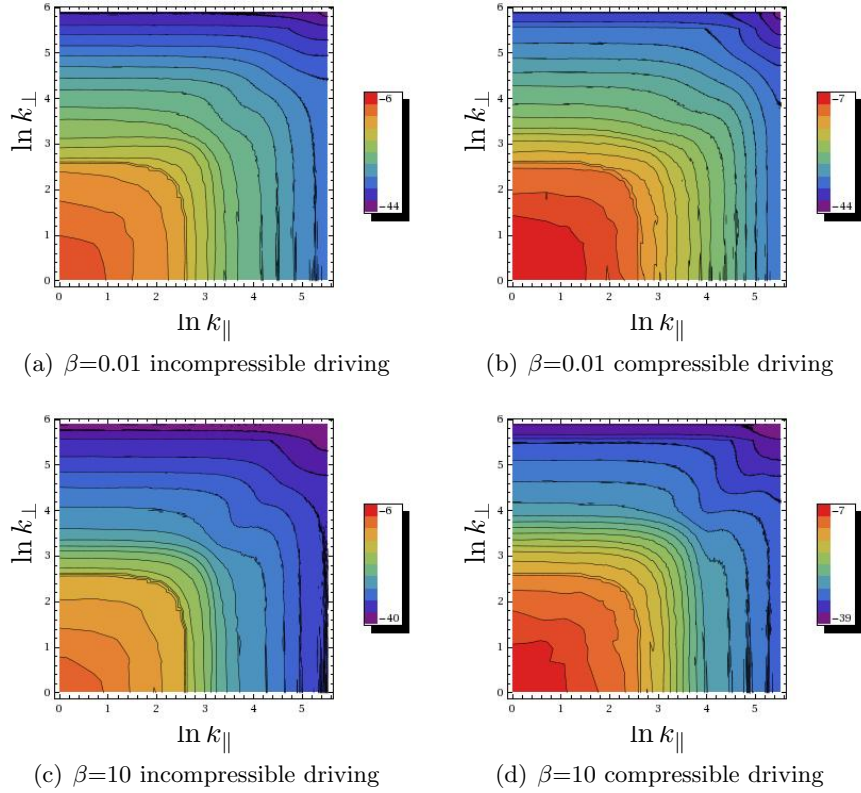


Figure 3: Turbulence spectra P_K after $t = 5 \cdot 10^3$ simulated on a 512^3 grid.

are anisotropic. The contour lines of a spectrum with a parallel preferred direction cross the axes for higher values of k_{\parallel} than k_{\perp} . For the contour lines of a spectrum with a perpendicular preferred direction it's the other way around. For $\beta=10$ we see for compressible as well as for incompressible driving a very homogeneous driving spectrum. This can be understood quite easily. We drive the turbulence with compressible or incompressible fluctuations in the velocity fields. As shown in chapter 4.1.1 this results in an excitation of MHD-waves in the driving range, so turbulent energy of the velocity fields is transferred into magnetic energy. In the direction of preferred excitation of waves this energy is missing in the velocity fields and so in P_K . This is why for the case of incompressible driving and $\beta = 0.01$ we find Alfvén waves propagating parallel to the mean magnetic field and so a perpendicular preferred direction in P_K . For compressible driving we excite fast magnetosonic waves perpendicular to the mean magnetic field which results in a parallel preferred direction of P_K .

For $\beta = 10$ although the same is in all likelihood happening this effect can't be seen, because the magnetic fields are much weaker and so less waves are excited and through this less energy of P_K is transformed into P_B . Hereby the missing energy in P_K in one of the preferred directions can't be detected in P_K .

4.1.3. P_{Shear} and P_{Comp}

Now we will investigate the two dimensional spectra of P_{Comp} and P_{Shear} . Figure 4(a) to 5(d) show the two dimensional spectra of P_{Comp} and P_{Shear} at a normalised time of $5 \cdot 10^{-3}$. At this very early time the type of driving dominates the turbulent energy of the velocity fields. So for $\beta = 0.01$ the driving component shows of cause the same behaviour as P_K for $\beta = 0.01$. We also find for compressible driving a parallel preferred direction in P_{Comp} ($k_{\perp}^{aniso}(2.2) = 2.0$) as in this case fast magnetosonic waves are generated propagation perpendicular to the mean magnetic field and this energy comes from the turbulent energy of the velocity components. For P_{Shear} and incompressible driving we find a perpendicular preferred direction ($k_{\perp}^{aniso}(1.4) = 1.8$), as we have an excitation of parallel propagating Alfvén waves. The non driven components - P_{Comp} for incompressible driving and P_{Shear} for compressible driving - show in principle the same diagonal symmetry. In chapter 2.3 it was shown that Alfvén waves can be generated via three wave interaction from fast magnetosonic waves propagating perpendicular to the mean magnetic field and that these Alfvén waves propagate with an angel of 45 degree to the fast magnetosonic waves. This prediction corresponds to the two dimensional spectrum of P_{Shear} for compressible driving. The same can be done for P_{Comp} and incompressible driving.

For $\beta = 10$ we find the same P_{Comp} and P_{Shear} limitations as for P_K : Because of the weak magnetic fields only few waves are generated and this effect becomes as little noticeable as in the driven component as in P_K . As the non-driven component is also absolutely isotropic, no clear conclusion about the dominating physical process can be made.

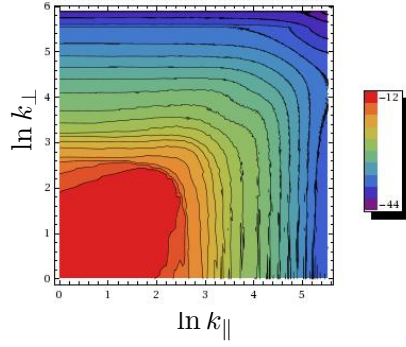
One should note that there should exist a connection between the P_{comp} results and the density fluctuations through the continuity equation. Density fluctuations have been studied in detail by Kowal *et al.* (2007), where only solenoidal driving is used.

4.2. Evolving spectrum

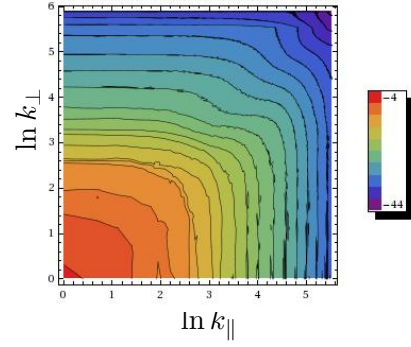
In the following chapter P_K, P_{Comp}, P_{Shear} and P_B for the four different setups are plotted against the normalised time (see figure 6(a) and 6(b) as well as figure 8(a) and 8(b)). It can be seen that there is no turbulent energy in the fields at the beginning of the simulation. As the turbulence is driven continuously through the whole simulation more and more turbulent kinetic energy is injected in the fields with time until at last the turbulence saturates (this is when the input energy from the driving is balanced by the numerical dissipation). A detailed analysis about the saturation range is given in section 4.3. Here we are mainly concerned about the physics before convergence is reached. The absolute amplitude of the energies in the convergence range is influenced by numerical effects and is so neglected in the discussion.

4.2.1. Turbulent kinetic energy P_K

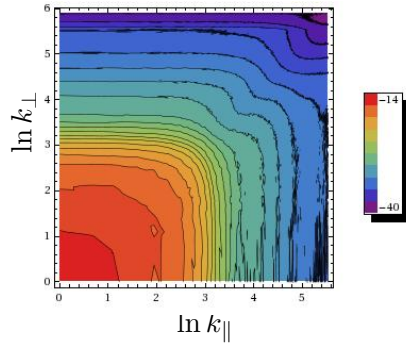
The temporal evolution of P_K differs fundamentally between compressible and incompressible driving (see figure 6(b)). This is especially apparent for $\beta = 10$. For com-



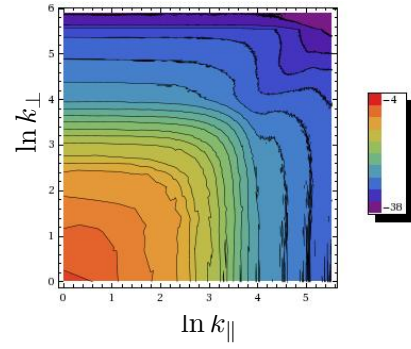
(a) $\beta=0.01$ incompressible driving



(b) $\beta=0.01$ compressible driving



(c) $\beta=10$ incompressible driving



(d) $\beta=10$ compressible driving

Figure 4: P_{Comp} after $t = 5 \cdot 10^{-3}$ simulated on a 512^3 grid.

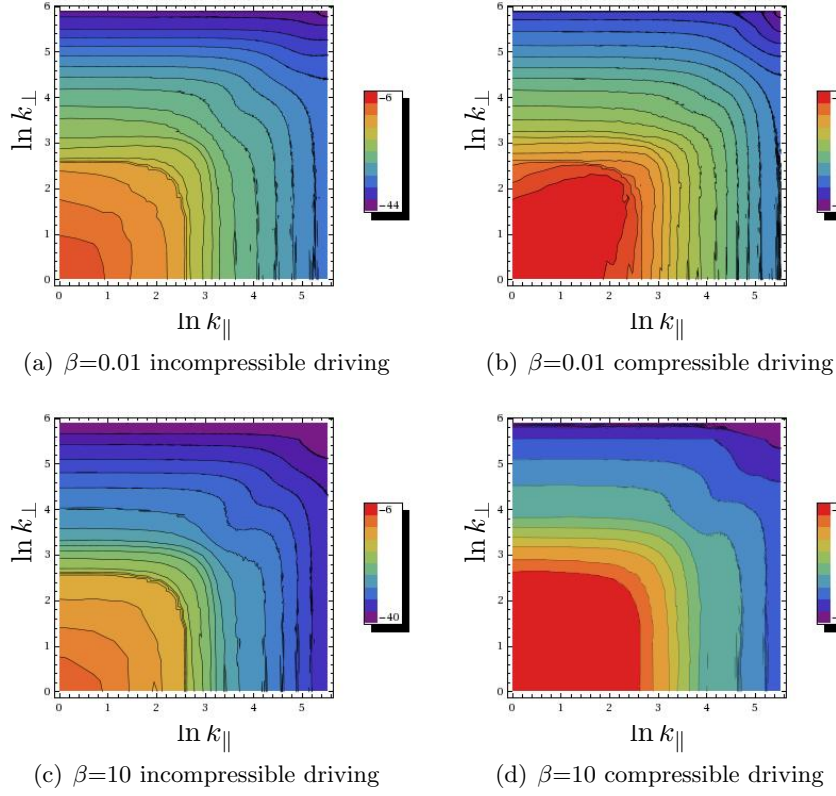


Figure 5: P_{Shear} after $t = 5 \cdot 10^{-3}$ simulated on a 512^3 grid.

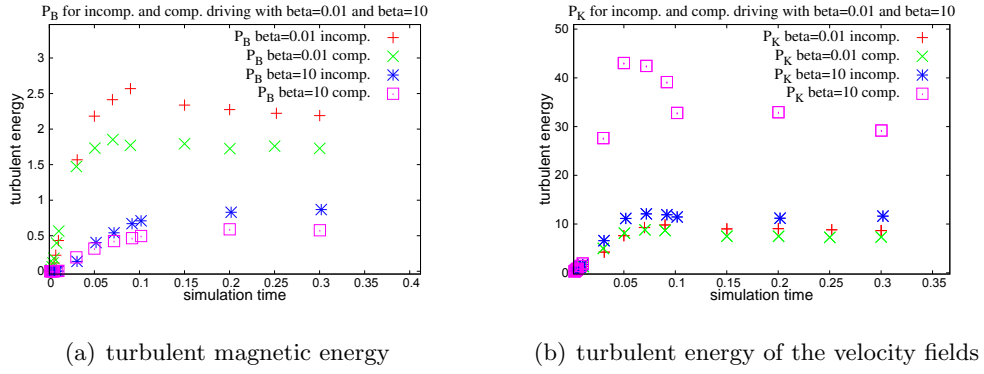


Figure 6: Turbulence spectra P_K and P_B as a function of the simulation time

compressible driving we find a distinct maximum for P_K at $t \simeq 0.05$. After that the energy decreases before finally saturation is reached.

What causes the formation of this maximum? In principle we find for both - compressible and incompressible fluctuations - the same behaviour: If the magnetic field lines are bent, the cascade and so the dissipation of the energy in the system is more efficient. From the data we can see that for compressible driving perpendicular fluctuations are generated that decay into the parallel direction which leads to an isotropic spectrum. To do this they need a component parallel to the background magnetic field. If the background field is quite tangled the fluctuations have a parallel component locally and can decay. For incompressible driving parallel fluctuations are generated that decay into perpendicular direction and so they need a perpendicular component to the background field. This is why they as well can only decay in a tangled field. The formation of the maximum can occur if the driving energy will bend the magnetic field lines only insufficiently. So for quite a long time there won't be a cascade and the resulting dissipation of the energy. Hereby lots of energy is accumulated until finally the field lines are bent enough to build up the cascade. Then the accumulated energy for small \vec{k} can at last be reduced by the cascade and the combined dissipation. If the driving energy bends the magnetic field lines efficiently from the beginning the cascade will build up from the beginning. Through this no energy is accumulated and no maximum will occur.

The magnetic field lines for compressible and incompressible driving at this maximum ($t=0.05$) and after convergence is reached are shown in figure 10(a) to 10(d). It can be seen that for the case of compressible driving the magnetic field lines are still quite smooth at the maximum whereas in the convergence range they are quite tangled. For the case of incompressible driving however the field lines are already quite tangled at $t=0.05$. This can be understood, when considering how the driving acts on the fluid. For a incompressible driving we are basically adding eddy-like motions to our fluid. This means that we get some shear-flows, which will certainly bend the background field lines. When adding a compressible velocity field, however, the background field even remains undisturbed for some of the input wave-modes. This shows, that an incompressible driving field will tangle the field lines much more efficiently. Thus, we find for $\beta = 10$ that with the incompressible driving field the field is tangled so early that such an energy storage as in the case of the compressible driving can not form at all.

This tangling of the magnetic field lines can also be accessed quantitatively. For this we computed the spatial averages of the quantity

$$a = 1 - 2\mu^2 \quad (27)$$

where μ is the angle between the local and the initial magnetic field. For this Parameter we find alignment along the initial magnetic field direction for $a = -1$, where a magnetic field that is perpendicular to the initial one would yield $a = 1$. Due to the fact that there is a higher degree of freedom for the perpendicular direction an isotropic distribution would yield $a = 1/3$. With this in mind we can discuss the results for our simulations.

For an initial plasma- β of $\beta = 0.01$ the alignment-parameter a even for the saturated turbulence at $t = 0.3$ never exceeds values of -0.9, which is still very parallel. For $\beta = 10$,

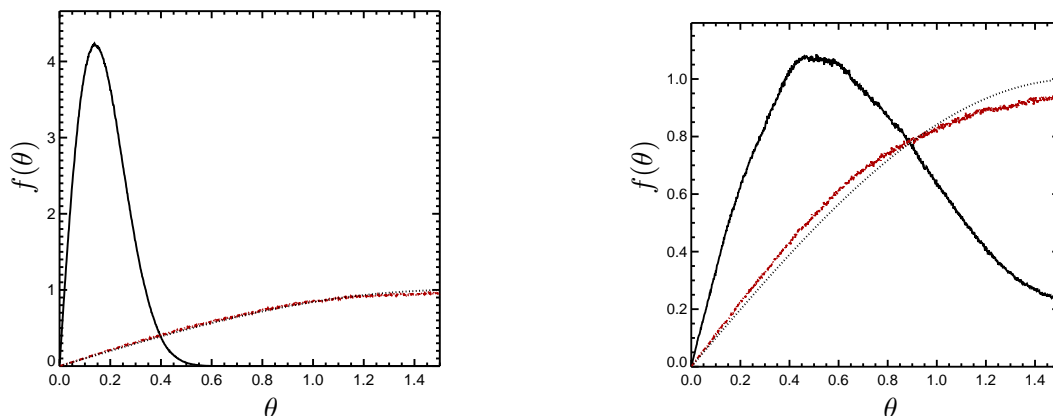


Figure 7: Distribution function of the magnetic field angle for different times and different numerical simulation runs – all results are shown for $\beta = 10$. On the left we show results for the incompressibly driven turbulence for $t = 0.01$ (black curve) and for $t = 0.3$ (red curve). On the right the results for compressible (black curve) and incompressible driving (red curve) are compared for $t = 0.05$. In both plots the dashed line indicates homogeneous distribution.

however, the situation is very different. In this case we find at $t = 0.05$ (which is the time, when the peak in the energy evolution is most prominent) on the one hand a nearly isotropic distribution with $a = 0.296$ for the incompressible driver. For compressible driving on the other hand we find $a = -0.158576$, where both of these simulations show isotropic distributions at $t = 0.3$. This shows that the compressibly driven simulations with $\beta = 10$ are the only ones, for which the tangling of the fieldlines still changes significantly between $t = 0.05$ and the saturated state. This is also illustrated by the distribution functions shown in Fig. 7 for some of the simulations with $\beta = 10$. On the left we show the distribution function for very early times, where the magnetic field is still pretty much aligned, and the distribution for the saturated state, which is obviously quite isotropic (here one has to take into account that an isotropic distribution in all spatial directions yields a distribution of the form $\sin \theta$ when projected from 3D to a $B_{\parallel} - B_{\perp}$ distribution-function). On the right we compare the situation for incompressible and compressible driving at the time of the maximum. Apparently the distribution is still much more aligned for the compressibly driven simulation.

In this context the simulations of Beresnyak & Lazarian (2009) should be mentioned: Taking into account a partially similar situation, they evaluate also multidimensional spectra, but they follow a different approach. While in this paper the global frame of reference is used (the axes are determined by the background magnetic field), they are using a local frame of reference. The discussion which of these two approaches is the best is tedious and maybe not helpful. Looking at Fig. 7 we see that there is a clear bending of field lines, which would suggest using the local frame. But in our opinion there are

two major drawbacks using the local frame: i) the definition of the local frame is not completely unique and may be governed by cutoff effects, ii) in the case of very weak turbulence local and global frame will be equivalent, while for very strong turbulence we may see differences in the local frame picture, which will in the end not affect the global picture (which is usually the one being observed).

4.2.2. P_B

For early times it can be seen that P_B has higher values for compressible than for incompressible driving (see figure 6(a) and table 1). This is due to the fact that for incompressible driving Alfvén waves are generated propagating in the x -direction whereas for compressible driving fast magnetosonic waves are generated propagating within the whole perpendicular y - z -plane. So the magnetosonic waves have an additional degree of freedom for their excitation and because of that more fast magnetosonic waves than Alfvén waves are excited for the same driving strength and driving time.

During the whole simulation much more turbulent energy of the velocity fields is converted into magnetic energy for small β than for high β . This is due to the fact that the background magnetic field is stronger for small plasma- β s which yields stronger magnetic fluctuations by tangling the velocity fields.

P_B sometimes also shows a maximum before it reaches the saturation range (e.g. for $\beta = 0.01$ and incompressible driving at 0.09 in figure 6(a)). But in this case it barely depends on the driving but on β . This is because the rate magnetic energy is converted from the velocity fields depends strongly on β . For $\beta = 10$ this rate is anyway so small that even a quite inefficient cascade is adequate to remove enough energy that no maximum can build up. For small β the energy is converted fast enough that in principle a maximum can build up. As for the case of incompressible driving more energy is converted in the saturation range the maximum is even slightly higher (see figure 6(a) for $\beta = 0.01$ and incompressible driving at 0.09 as well as for $\beta = 0.01$ and compressible driving at 0.075).

4.2.3. P_{Shear} and P_{Comp}

P_{Shear} and P_{Comp} are plotted in 8(a) to 8(b) and 9(a) to 9(d) together with the total energy of the velocity fields P_K . In table 2 the energies are listed for a normalised time of $5 \cdot 10^{-3}$ and for the saturated state of the spectrum.

At the beginning of the simulation the energy of the driving component is higher for $\beta = 10$ than for $\beta = 0.01$. This is because for bigger plasma- β s there are smaller magnetic fields and consequently less waves are generated. So less energy of the driving component is transformed into magnetic energy and hence missing in the energy of the driving component. Additionally as there are less excited modes for $\beta = 10$ the non driven component is smaller because less modes are generated that can decay into other waves and so transform compressible modes into incompressible modes and the other way around.

Whereas the driving dominates P_K in the beginning it stands out that the incompressible

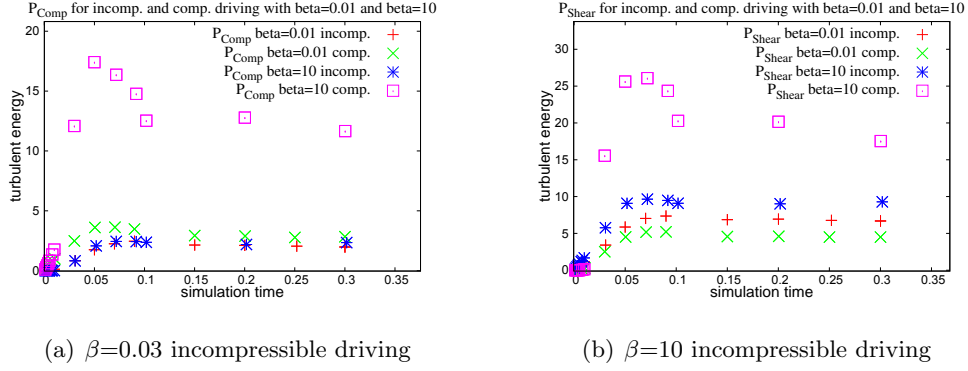


Figure 8: Turbulence spectra P_{Comp} and P_{Shear} as a function of the simulation time

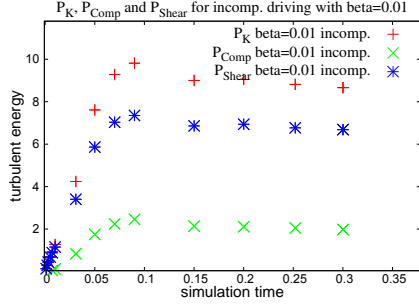
	driving	β	PB	PK	$\frac{PB}{PK}$
time 0.05	incomp.	0.01	$9.2769 \cdot 10^{-3}$	0.6986	0.0133
time 0.05	comp.	0.01	0.014504	0.70617	0.0205
time 0.05	incomp.	10	$1.9613 \cdot 10^{-5}$	0.81475	$2.407 \cdot 10^{-5}$
time 0.05	comp.	10	$5.042 \cdot 10^{-5}$	0.828	$6.089 \cdot 10^{-5}$
saturation	incomp.	0.01	0.177	8.84	0.02
saturation	comp.	0.01	0.1383	7.363	0.0188
saturation	incomp.	10	0.0675	11.42	$5.913 \cdot 10^{-3}$
saturation	comp.	10	0.0465	31.05	$1.502 \cdot 10^{-3}$

Table 1: magnetisation of the system.

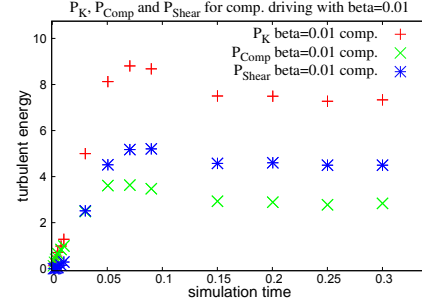
energy after some time dominates P_K independently of the kind of driving and the plasma- β . The dominance of the incompressible energy might be caused by a more efficient conversion of compressible modes into incompressible modes than the other way around. The saturated results given in chapter 4.3 support this idea.

4.3. Saturated state of the spectrum

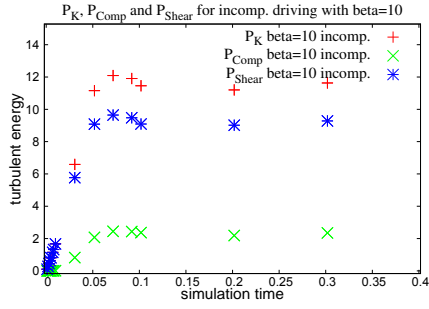
The saturated state of the spectrum has been described in a number of previous papers. In the work of Cho & Lazarian (2002, 2003). While Cho & Lazarian (2002) concentrated on the simulation of low- β plasmas, Cho & Lazarian (2003) also considered high- β plasmas. In both cases incompressible driving was used. As discussed above we will also use compressible driving, which may be motivated by supernova shock waves driving the ISM. Another point which is different is that the authors of the aforementioned studies attempted the decomposition into different wave modes. Our approach will focus on the decomposition in irrotational and solenoidal fields. This is specifically useful when one



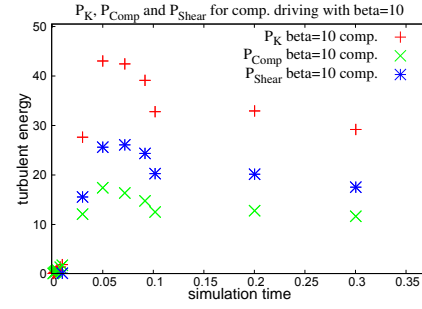
(a) $\beta=0.01$ incompressible driving



(b) $\beta=0.01$ compressible driving



(c) $\beta=10$ incompressible driving

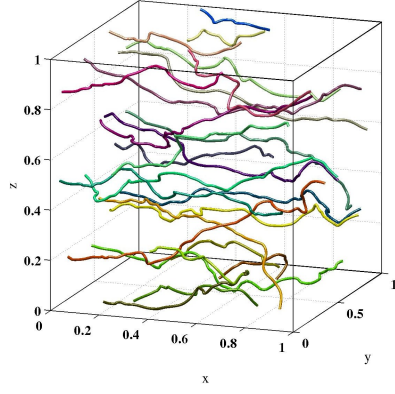


(d) $\beta=10$ compressible driving

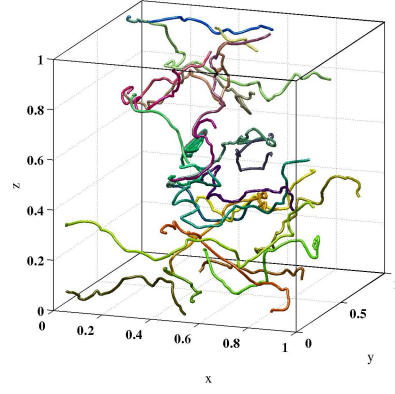
Figure 9: Total turbulent energies P_K, P_{Comp} and P_{Shear} as a function of the simulation time

	driving	β	PShear	PComp	$\frac{P_{Comp}}{P_{Shear}}$
time 0.05	incomp.	0.01	0.676	0.022	$3.25 \cdot 10^{-2}$
time 0.05	comp.	0.01	0.0521	0.654	12.55
time 0.05	incomp.	10	0.814	$3.19 \cdot 10^{-4}$	$3.92 \cdot 10^{-4}$
time 0.05	comp.	10	$6.47 \cdot 10^{-3}$	0.822	127.0
saturation	incomp.	0.01	6.80	2.03	0.30
saturation	comp.	0.01	4.53	2.82	0.62
saturation	incomp.	10	9.14	2.27	0.25
saturation	comp.	10	18.86	12.2	0.65

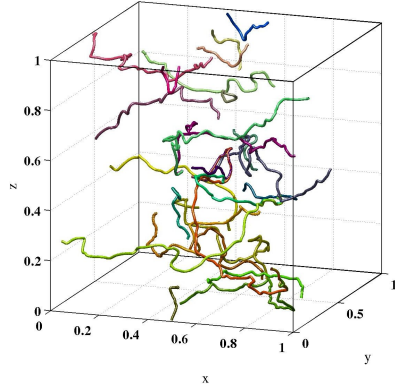
Table 2: compressible and incompressible energy of the system.



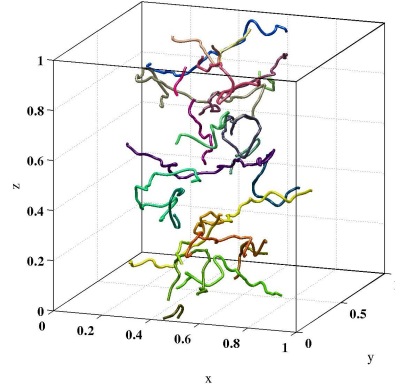
(a) magnetic field lines for $\beta = 10$ with compressible driving after $t=0.05$



(b) magnetic field lines for $\beta = 10$ with compressible driving after $t=0.3$



(c) magnetic field lines for $\beta = 10$ with incompressible driving after $t=0.05$



(d) magnetic field lines for $\beta = 10$ with incompressible driving after $t=0.3$

Figure 10: Magnetic field lines for $\beta = 10$ with compressible and incompressible driving

assumes that the turbulence is dominated by shocks.

Here we present the two dimensional spectra for the saturated state of the turbulence. For $\beta = 0.01$ and compressible driving P_K , P_{Shear} and P_{Comp} have a clearly parallel preferred direction (see figure 12(b), 13(b) and 14(b)). In the saturated state we are concerned with fully nonlinear interactions, which form an anisotropic cascade, as we see from the results. For incompressible driving we find that P_K and P_{Shear} develop a perpendicular preferred direction (see figure 12(a) and 13(a)), as it has been predicted by Shebalin *et al.* (1983). The spectrum of P_{Comp} however is quite isotropic (see figure 14(a)). As it has been already mentioned in chapter 4.2.3, we believe that compressible modes may easily be converted into incompressible modes, but not the other way around. This is confirmed by the two dimensional spectra, because for compressible driving P_{Shear} has the same anisotropy as P_{Comp} . Actually the incompressible modes would build up a perpendicular cascade as can be seen by the results in 12(a) and 13(a), as they are however directly generated by the compressible modes, the cascade is forced to build up the same preferred direction. Contrariwise in the case of incompressible driving P_{Comp} has not the same preferred direction as P_{Shear} . So the transformation of compressible modes from incompressible modes is not that efficient. This is why a superposition of compressible and incompressible modes and so of a parallel and perpendicular cascade can be seen. The result is an isotropic spectrum.

For $\beta = 0.01$ it can be seen that for incompressible driving P_B has the same perpendicular preferred direction that we also find for P_K , P_{Shear} (see figure 11(a)) whereas for compressible driving there is no preferred direction (see figure 11(b)). In figure 9(a) it can be seen that for incompressible driving much more incompressible modes than compressible modes are in the system. This is why we would also expect a perpendicular cascade to build up. For the case of compressible driving (see figure 9(b)) we have only slightly more incompressible than compressible modes in the system. In this case the magnetic energy will cascade in parallel and perpendicular direction. One requirement is that magnetic and kinetic energy may cascade differently. The spectra suggest that this is indeed what happens in the simulations, but an explanation is hard.

For $\beta = 10$ the two dimensional spectra are quite isotropic as we would predict it for a this widely hydrodynamical case (see figure 11(c), 11(d), 12(c), 12(d), 13(c), 13(d), 14(c) and 14(d)).

Similar investigations have been done by Vestuto *et al.* (2003) for the case of incompressible driving in the saturated state of the spectrum. He also found a perpendicular preference of the fluctuations for small values of the plasma- β , which disappears for higher β .

5. Discussion

In this paper we presented results from simulations of compressible MHD turbulence for low- and high-beta plasmas with compressible and incompressible driving. Our special focus was on the evolution of the turbulence. We found an obvious influence of the plasma- β and the type of driving on the anisotropy and the temporal energy evolution.

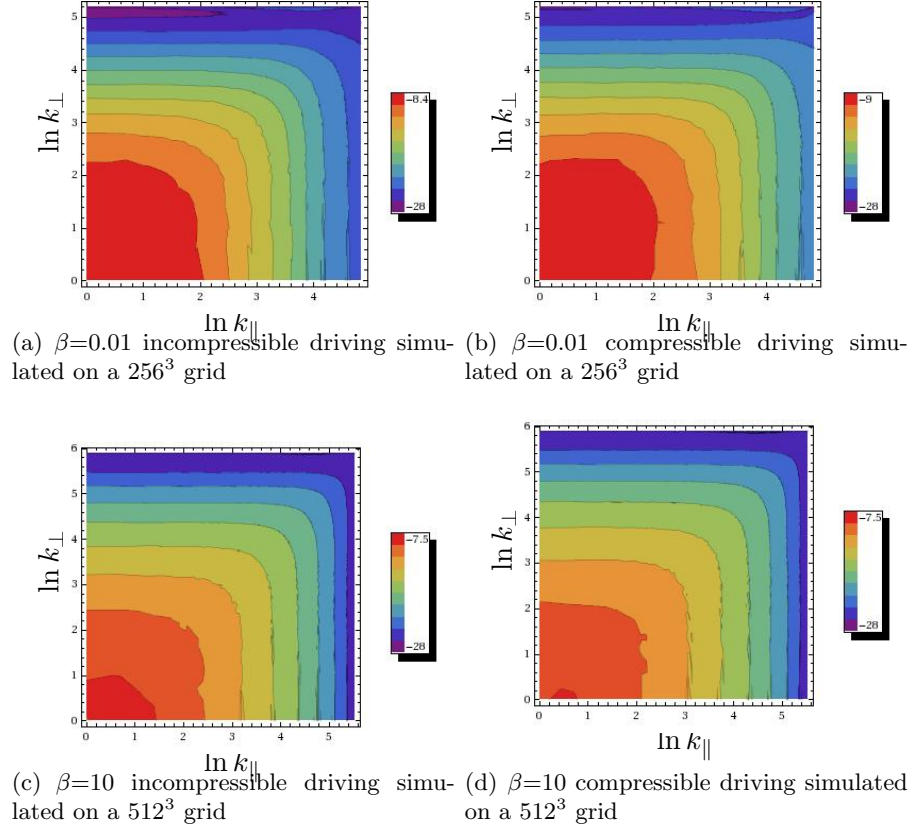


Figure 11: P_B in the saturated state of the turbulence simulated on a 256^3 and a 512^3 grid.

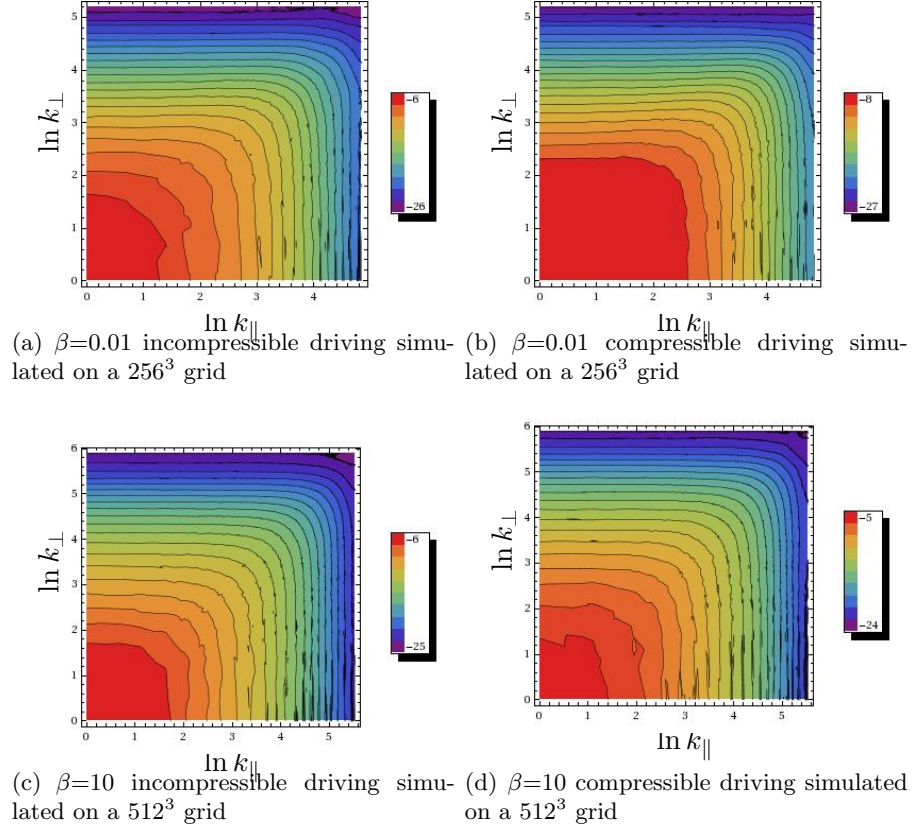


Figure 12: P_K in the saturated state of the turbulence simulated on a 256^3 and a 512^3 grid.

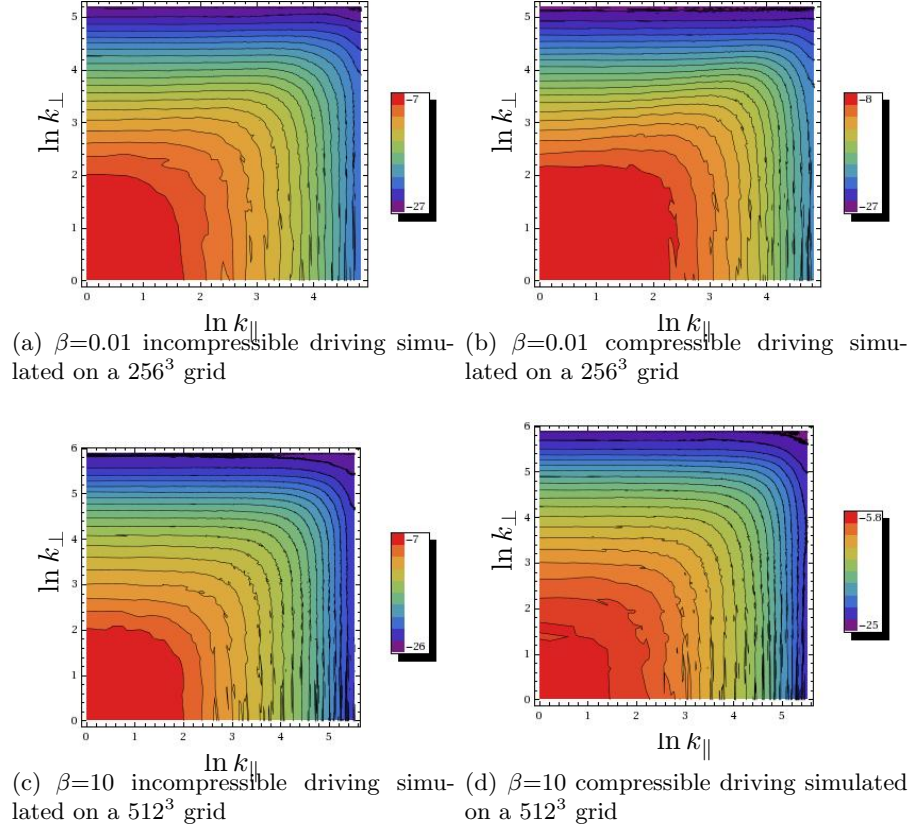


Figure 13: P_{Shear} in the saturated state of the turbulence simulated on a 256^3 and a 512^3 grid.

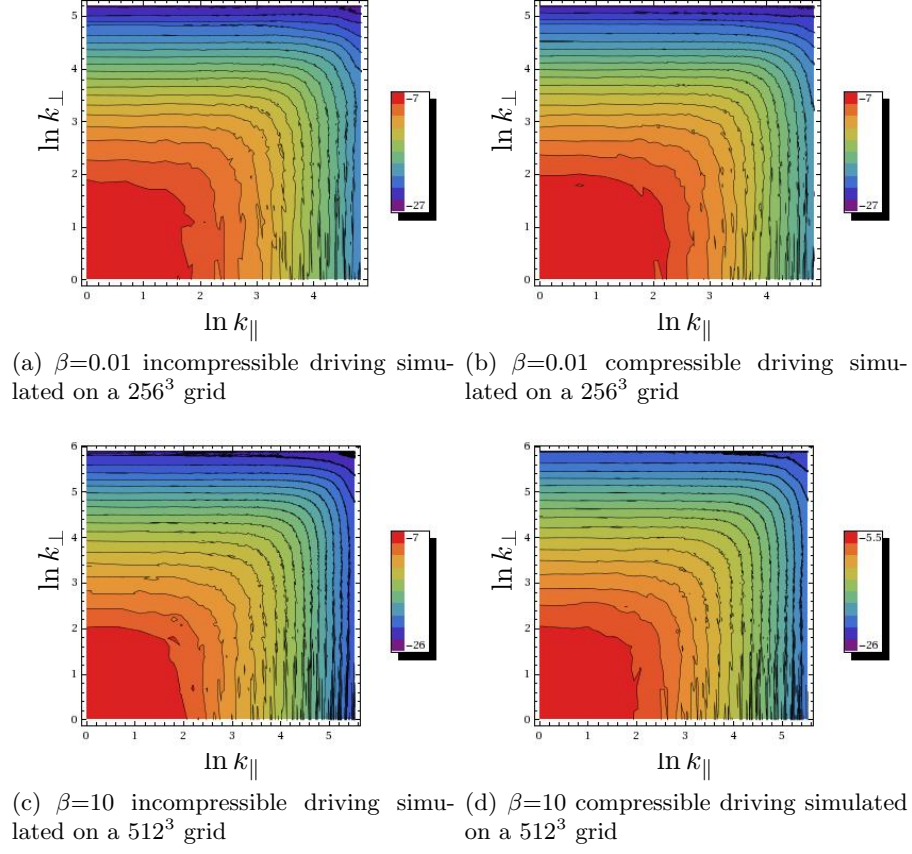


Figure 14: P_{Comp} in the saturated state of the turbulence simulated on a 256^3 and a 512^3 grid.

Especially the influence of the driver has not yet been discussed for MHD plasmas so far.

This may have influence on a number of astrophysical scenarios. When assuming supernovae as energy input, it is evident that e.g. the pile-up of fluctuation-energy due to slow tangling of magnetic field lines may be observed in the early stages as a lower temperature of the plasma. So by observing temperature evolution in turbulent driving it should be possible to determine which process is really driving the turbulence: Incompressible or compressible fluctuations.

Even more striking is the influence on particle acceleration in evolving turbulence. Here also early supernova remnants are the object of interest. The first thing to observe here, is that a weak cascade in compressible driving may prevent low energetic particles to be accelerated due to missing energy at their respective resonant high wavenumbers.

It is not completely clear if the anisotropy arising in first place will have an observable effect, but it is very well possible that the anisotropy in the magnetic fluctuations may change the transport and consecutively the acceleration and escape of cosmic ray from turbulent regions.

6. Summary

This paper gave summary of the evolution of turbulence in a driven MHD plasma. The evolution is described especially under the influence of different driving mechanisms (compressible and incompressible). First principles are able to explain the spectra for the very early development of turbulence. The anisotropy of wave generation is able to explain the specific features visible. For the further development of turbulence the plasma beta plays an essential role in the saturation of the spectra. We have shown the distribution of energy between magnetic and kinetic energy depending on the plasma beta. The results shown here are in agreement with earlier research done for hydrodynamics and goes into more detail regarding the specific anisotropy introduced with the background field.

Acknowledgements

MW acknowledges support by Graduiertenkolleg 1147 and FS acknowledges support by *Deutsche Forschungsgemeinschaft, DFG* project number Sp 1124/3.

We would like to thank the anonymous referee for his detailed comments, which helped improving this paper.

A. Measure of the anisotropy

Anisotropy is one of the main features discussed in the context of this paper. The qualitative behaviour of the anisotropy can be seen in the two-dimension plots of the spec-

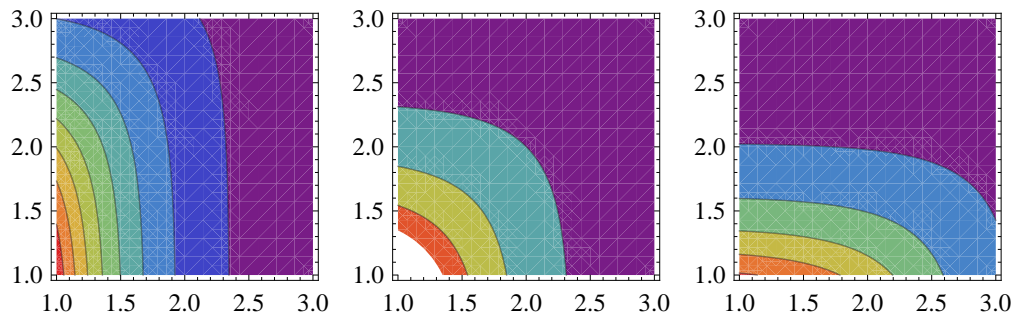


Figure 15: Two-dimensional spectra for the sample spectrum Eq. 28. Shown are plots for the values of $\Lambda = 0.1, 1, 10$.

trum. A quantitative description is far more difficult since the actual shape of the two-dimensional spectra may differ strongly.

To give a rough quantitative comparison we are trying to boil down the plot to single numbers. We are using the contour lines to find a $k_{\perp}^{\text{aniso}}(k_{\parallel})$. By following a contour line starting at a given value of k_{\parallel} from the k_{\parallel} axis to the k_{\perp} axis we find this parameter.

We want to illustrate the determination with a sample anisotropic function

$$f(x, y) = \frac{1}{(x^2 + \Lambda y^2)^{\frac{5}{3}12}} \quad (28)$$

The contour plots for different parameters Λ are shown in Fig. 15. For the simple case of $\Lambda = 1$ we find for example $k_{\perp}^{\text{aniso}}(2.3) = 2.3$. The ratio of k_{\parallel} and k_{\perp} is here 1, since the function is anisotropic. For $\Lambda = 0.1$ we find $k_{\perp}^{\text{aniso}}(1.7) = 2.7$ and for $\Lambda = 10$ we find $k_{\perp}^{\text{aniso}}(2.6) = 1.6$.

This number gives a first quantitative hint on the anisotropy of the problem, but it is limited to axis aligned asymmetry. For feature propagating at 45 degree to the magnetic field it does not show any features.

References

- ARMSTRONG, J. W., RICKETT, B. J. & SPANGLER, S. R. 1995 Electron density power spectrum in the local interstellar medium. *Astrophys. J.* **443**, 209–221.
- BERESNYAK, A. & LAZARIAN, A. 2009 Comparison of Spectral Slopes of Magnetohydrodynamic and Hydrodynamic Turbulence and Measurements of Alignment Effects. *Astrophys. J.* **702**, 1190–1198.
- CHANDRAN, B. D. G. 2005 Weak Compressible Magnetohydrodynamic Turbulence in the Solar Corona. *Physical Review Letters* **95** (26), 265004–+.
- CHANDRAN, B. D. G. 2008 Weakly Turbulent Magnetohydrodynamic Waves in Compressible Low- β Plasmas. *Physical Review Letters* **101** (23), 235004–+.

- CHERNYSHOV, A. A., KARELSKY, K. V. & PETROSYAN, A. S. 2007 Development of large eddy simulation for modeling of decaying compressible magnetohydrodynamic turbulence. *Physics of Fluids* **19** (5), 055106–+.
- CHERNYSHOV, A. A., KARELSKY, K. V. & PETROSYAN, A. S. 2009 Validation of large eddy simulation method for study of flatness and skewness of decaying compressible magnetohydrodynamic turbulence. *Theoretical and Computational Fluid Dynamics* **23**, 451–470.
- CHIN, Y.-C. & WENTZEL, D. G. 1972 Nonlinear Dissipation of Alfvén Waves. *Astrophys. Space. Sci.* **16**, 465–477.
- CHO, J. & LAZARIAN, A. 2002 Compressible Sub-Alfvénic MHD Turbulence in Low- β Plasmas. *Physical Review Letters* **88** (24), 245001–+.
- CHO, J. & LAZARIAN, A. 2003 Compressible magnetohydrodynamic turbulence: mode coupling, scaling relations, anisotropy, viscosity-damped regime and astrophysical implications. *Mon. Not. R. Astron. Soc.* **345**, 325–339.
- CHO, J. & VISHNIAC, E. T. 2000 The Anisotropy of Magnetohydrodynamic Alfvénic Turbulence. *Astrophys. J.* **539**, 273–282.
- ELMEGREEN, B. G. & SCALO, J. 2004 Interstellar Turbulence I: Observations and Processes. *Ann. Rev. Astron. Astrophys.* **42**, 211–273.
- FEDERRATH, C., CHABRIER, G., SCHOBER, J., BANERJEE, R., KLESSEN, R. S. & SCHLEICHER, D. R. G. 2011 Mach Number Dependence of Turbulent Magnetic Field Amplification: Solenoidal versus Compressive Flows. *Physical Review Letters* **107** (11), 114504.
- FEDERRATH, C., KLESSEN, R. S. & SCHMIDT, W. 2008 The Density Probability Distribution in Compressible Isothermal Turbulence: Solenoidal versus Compressive Forcing. *Astrophys. J., Lett.* **688**, L79–L82.
- FEDERRATH, C., ROMAN-DUVAL, J., KLESSEN, R. S., SCHMIDT, W. & MAC LOW, M.-M. 2010 Comparing the statistics of interstellar turbulence in simulations and observations. Solenoidal versus compressive turbulence forcing. *Astron. Astrophys.* **512**, A81+.
- FRISCH, U. 1995 *Turbulence. The legacy of A. N. Kolmogorov.*
- GOLDREICH, P. & SRIDHAR, S. 1995 Toward a theory of interstellar turbulence. 2: Strong alfvénic turbulence. *Astrophys. J.* **438**, 763–775.
- GRAUER, R., KRUG, J. & MARLIANI, C. 1994 Scaling of high-order structure functions in magnetohydrodynamic turbulence. *Physics Letters A* **195**, 335–338.

- HAVERKORN, M., KATGERT, P. & DE BRUYN, A. G. 2004 Structure in the polarized Galactic synchrotron emission, in particular “depolarization canals”. *Astron. Astrophys.* **427**, 549–559.
- KLESSEN, R. S. 2000 One-Point Probability Distribution Functions of Supersonic Turbulent Flows in Self-gravitating Media. *Astrophys. J.* **535**, 869–886.
- KOLMOGOROV, A. 1941 The Local Structure of Turbulence in Incompressible Viscous Fluid for Very Large Reynolds’ Numbers. *Akademiia Nauk SSSR Doklady* **30**, 301–305.
- KOWAL, G., LAZARIAN, A. & BERESNYAK, A. 2007 Density Fluctuations in MHD Turbulence: Spectra, Intermittency, and Topology. *Astrophys. J.* **658**, 423–445.
- KURGANOV, A. & LEVY, D. 2000 A Third-Order Semi-Discrete Central Scheme for Conservation Laws and Convection-Diffusion Equations. *ArXiv Mathematics e-prints*.
- KUZNETSOV, E. A. 2001 Weak Magnetohydrodynamic Turbulence of a Magnetized Plasma. *Soviet Journal of Experimental and Theoretical Physics* **93**, 1052–1064.
- LAZAR, M., SPANIER, F. & SCHLICKEISER, R. 2003 Linear damping and energy dissipation of shear Alfvén waves in the interstellar medium. *Astron. Astrophys.* **410**, 415–424.
- LAZARIAN, A. & POGOSYAN, D. 1997 Interstellar Filaments and the Statistics of Galactic H i. *Astrophys. J.* **491**, 200–+.
- LEMASTER, M. N. & STONE, J. M. 2009 Dissipation and Heating in Supersonic Hydrodynamic and MHD Turbulence. *Astrophys. J.* **691**, 1092–1108.
- LITHWICK, Y. & GOLDBREICH, P. 2001 Compressible Magnetohydrodynamic Turbulence in Interstellar Plasmas. *apj* **562**, 279–296.
- MARON, J. & GOLDBREICH, P. 2001 Simulations of Incompressible Magnetohydrodynamic Turbulence. *Astrophys. J.* **554**, 1175–1196.
- PADOAN, P., JUVELA, M., KRITSUK, A. & NORMAN, M. L. 2006 The Power Spectrum of Supersonic Turbulence in Perseus. *Astrophys. J., Lett.* **653**, L125–L128.
- POLITANO, H. & POUQUET, A. 1995 Model of intermittency in magnetohydrodynamic turbulence. *pre* **52**, 636–641.
- SHE, Z.-S. & LEVEQUE, E. 1994 Universal scaling laws in fully developed turbulence. *Physical Review Letters* **72**, 336–339.
- SHEBALIN, J. V., MATTHAEUS, W. H. & MONTGOMERY, D. 1983 Anisotropy in MHD turbulence due to a mean magnetic field. *Journal of Plasma Physics* **29**, 525–547.
- SKILLING, J. 1975 Cosmic ray streaming. III - Self-consistent solutions. *Mon. Not. R. Astron. Soc.* **173**, 255–269.

- SPANIER, F. & SCHLICKEISER, R. 2005 Damping and wave energy dissipation in the interstellar medium. II. Fast magnetosonic waves. *Astron. Astrophys.* **436**, 9–16.
- SRIDHAR, S. & GOLDBREICH, P. 1994 Toward a theory of interstellar turbulence. 1: Weak Alfvénic turbulence. *Astrophys. J.* **432**, 612–621.
- VAINIO, R. & SPANIER, F. 2005 Evolution of Alfvén waves by three-wave interactions in super-Alfvénic shocks. *Astron. Astrophys.* **437**, 1–8.
- VESTUTO, J. G., OSTRICKER, E. C. & STONE, J. M. 2003 Spectral Properties of Compressible Magnetohydrodynamic Turbulence from Numerical Simulations. *Astrophys. J.* **590**, 858–873.
- VON WEIZSÄCKER, C. F. 1951 The Evolution of Galaxies and Stars. *Astrophys. J.* **114**, 165–+.